

# Ultrafast sublattice pseudospin relaxation in graphene probed by polarization-resolved photoluminescence

Thomas Danz, Andreas Neff,<sup>\*</sup> John H. Gaida, Reiner Bormann, Claus Ropers, and Sascha Schäfer<sup>†</sup>

*4th Physical Institute – Solids and Nanostructures, University of Göttingen, Göttingen, Germany*

(Received 24 January 2017; published 30 June 2017)

Electronic pseudospin degrees of freedom in two-dimensional materials exhibit unique carrier-field interactions which allow for advanced control strategies. Here, we investigate ultrafast sublattice pseudospin relaxation in graphene by means of polarization-resolved photoluminescence spectroscopy. A comparison with microscopic Boltzmann simulations allows us to determine a lifetime of the optically aligned pseudospin distribution of  $12 \pm 2$  fs. This experimental approach extends the toolbox of graphene pseudospintrronics, providing additional means to investigate pseudospin dynamics in active devices or under external fields.

DOI: 10.1103/PhysRevB.95.241412

Present-day electronic devices process, store, and transport information based on charge carriers. Recent developments in spintronics [1–3] have extended these capabilities by additionally making use of the electronic spin. Moreover, depending on the local environment, carriers can be equipped with additional pseudospin degrees of freedom, including sublattice, valley, and layer pseudospins, each exhibiting rich physical phenomena not unlike the ones observed for the intrinsic spin of electrons, and leading to possible applications in future information technology [4–7]. For example, the valley pseudospin is exploited in valleytronics [7] by manipulating the occupation of degenerate but inequivalent chiral electron states. In particular, in hexagonal two-dimensional (2D) materials such as transition metal dichalcogenides (TMDCs), selection rules enable a direct optical manipulation of the carrier pseudospin [6–10]. Manifestations of valley pseudospin polarization in TMDCs include the valley-spin analogs of the spin Hall effect [10,11] and the Zeeman effect [12].

Even single-layer graphene as the most simple 2D material displays valley and sublattice pseudospins [13]. Similar to the case of TMDCs, the valley pseudospin distinguishes the occupation within the Dirac cones at the  $K$  and  $K'$  points, and the sublattice pseudospin controls the relative phase of the electron wave function on the two hexagonal sublattices [14]. In momentum space, the sublattice pseudospin is collinear with the carrier momentum relative to the Dirac point [4,13]. For example, sublattice pseudospin conservation enables Klein tunneling, i.e., the counterintuitive carrier transmission through infinitely high potential barriers [15–17].

Also the coupling between carriers and optical fields [18] is governed by sublattice pseudospin selection rules [19], so that the initial carrier populations created by linearly polarized interband excitations exhibit a pronounced angularly asymmetric population within the Dirac cones [20]. However, intrinsic carrier scattering mechanisms are expected to rapidly destroy the optically imprinted pseudospin alignment. Ultrafast pseudospin relaxation has been addressed in a series of polarization-resolved transient optical spectroscopy

experiments [21–28], elucidating the role of carrier momentum isotropization in thermalization and cooling processes [29–38]. Although it is challenging to observe the fastest relaxation dynamics, most of the previous investigations suggest that sublattice pseudospin relaxation is complete within 50–150 fs [22–24]. Theoretical models predict even faster dynamics [39], and a precise relation between energetic and momentum relaxation time scales has not yet been established experimentally.

Here, we present evidence for a transient sublattice pseudospin alignment in graphene, obtained by analyzing the polarization-resolved photoluminescence (PL) from optically induced nonequilibrium carrier populations [40–43]. Comparing the experimentally observed PL polarization with microscopic simulations of Boltzmann rate equations, we demonstrate that the initial pseudospin alignment is lost within  $12 \pm 2$  fs. The results highlight the importance of efficient pseudospin relaxation in graphene, proceeding equally fast as energetic carrier thermalization, and an order of magnitude faster than the excitation of strongly coupled optical phonons [44].

In our experiments, single-layer graphene on a sapphire substrate is optically excited using ultrashort laser pulses (18 fs pulse duration, 1.55 eV photon energy, 80 MHz repetition rate). The resulting blueshifted PL is detected in a polarization-resolved manner by a grating spectrometer and a liquid-nitrogen-cooled charge-coupled device (CCD). At the excitation conditions employed, no optically induced sample damage was observed, and special care was taken to ensure accurate calibration of the spectral and polarization responses of the detection system (see Supplemental Material [45]).

Figure 1(a) schematically depicts the experimental setup and the microscopic processes underlying the PL emission. Ultrashort, linearly polarized optical pump pulses excite carriers from the valence into the conduction band of graphene (red arrow). Initially, the nonequilibrium carrier distribution is strongly anisotropic within each Dirac cone of the graphene band structure [39]. During relaxation, carrier-carrier and carrier-phonon scatterings cause an energetic broadening of the carrier distribution and a loss of momentum anisotropy (black arrows). The emerging high-energy tail of the carrier distribution gives rise to a blueshifted component of the PL by electron-hole recombination (blue arrow), as previously

<sup>\*</sup>Present address: Leibniz Institute of Surface Modification, Leipzig, Germany.

<sup>†</sup>schaef@ph4.physik.uni-goettingen.de

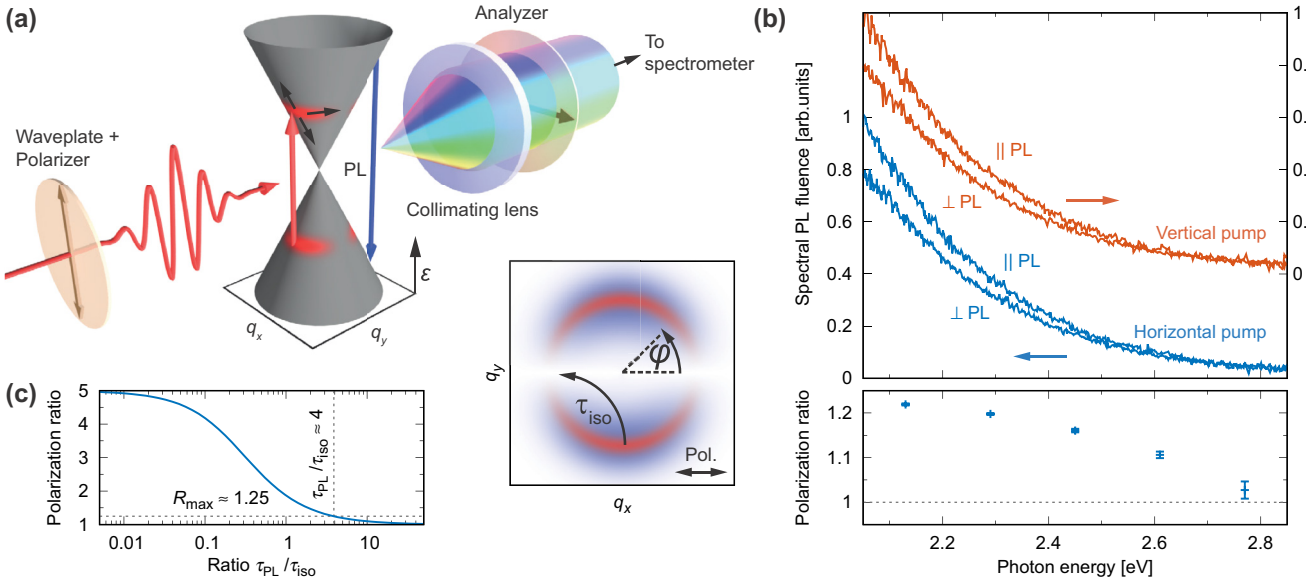


FIG. 1. (a) Schematics of the experimental setup and PL emission process. Horizontally or vertically polarized ultrashort pump pulses trigger carrier dynamics around the Fermi energy of graphene. The resulting hot-carrier PL is collimated and recorded as a function of photon energy and polarization (horizontal or vertical). Inset: Projection of the initial (red) and broadened (blue) momentum distribution after  $x$ -polarized optical excitation (see arrow) onto the  $q$  plane (momentum  $q$  relative to the  $K$  and  $K'$  points). The phenomenological azimuthal momentum randomization time scale  $\tau_{\text{iso}}$  is introduced. (b) Top: Representative spectra of parallel PL ( $\parallel$  PL) and perpendicular PL ( $\perp$  PL) for horizontal and vertical pump polarizations. The anisotropic nature of the PL emission is readily visible ( $117 \mu\text{J}/\text{cm}^2$  incident fluence). Bottom: Polarization ratios extracted from the PL spectra above (averaged over both pump polarizations,  $0.16 \text{ eV}$  bin width). (c) Polarization ratio as a function of  $\tau_{\text{PL}}/\tau_{\text{iso}}$  in a model of two coupled, exponentially decaying carrier populations  $\parallel$  and  $\perp$ . The indicated value of  $R_{\text{max}} \approx 1.25$  is the maximum polarization ratio observed in the experiment according to the data in (b).

observed [40–42], with recombining carriers at an energy  $\pm\varepsilon$  emitting a PL photon of energy  $E = 2\varepsilon$ . The carrier and phonon systems jointly thermalize due to an efficient energy transfer between carriers and a set of high-energy, strongly coupled optical phonons (SCOPs) on a hundred femtosecond time scale [33,44]. The SCOPs in turn decay on a time scale on the order of a picosecond [46–49].

In a phenomenological description, the PL lifetime and the azimuthal momentum randomization in the high-energy tail of the broadened carrier distribution can be characterized by two time scales  $\tau_{\text{PL}}$  and  $\tau_{\text{iso}}$ , respectively [see the inset in Fig. 1(a)]. Our experiments yield access to momentum and energy relaxation rates as the degree of PL polarization is governed by the ratio of these time constants. Specifically, in the limiting case of  $\tau_{\text{PL}} \gg \tau_{\text{iso}}$ , completely unpolarized PL emission is expected, whereas  $\tau_{\text{PL}} \lesssim \tau_{\text{iso}}$  would result in a PL preferentially polarized parallel to the pump.

Representative PL spectra obtained in our experiments are depicted in Fig. 1(b). The PL intensity decreases monotonously over the observed photon energy range in a spectral shape that was previously described by blackbody radiation [40]. Most importantly, the intensity of the PL polarized parallel to the pump (indicated by  $\parallel$ ) is up to 20% higher than the intensity of the perpendicular PL component (indicated by  $\perp$ ), evidencing considerable azimuthal carrier anisotropy within the PL lifetime. The agreement of the spectra for both horizontally (blue curves) and vertically (red curves) polarized pump beams demonstrates a proper polarization-dependent calibration of the detection. In order to quantify the PL

polarization properties, we employ a polarization ratio

$$R(E) = \frac{I_{\parallel}(E)}{I_{\perp}(E)} \quad (1)$$

of the temporally integrated PL flux,  $I_{\parallel}$  and  $I_{\perp}$ , polarized parallel and perpendicular to the pump, respectively, as a function of the photon energy  $E$ . Unpolarized PL emission corresponds to  $R = 1$ , while fully polarized PL emission is represented by  $R \rightarrow \infty$ .

To obtain a connection between the expected PL polarization and the introduced time constants, we describe the azimuthal and energetic carrier relaxation in a simplified model by two coupled, exponentially decaying components  $f_{c,\parallel}$  and  $f_{c,\perp}$  of the relevant high-energy carrier population in the conduction band,

$$\frac{df_{c,\parallel}}{dt} = -\frac{f_{c,\parallel}}{\tau_{\text{rel}}} - \frac{f_{c,\parallel} - f_{c,\perp}}{\tau_{\text{iso}}}, \quad (2)$$

$$\frac{df_{c,\perp}}{dt} = -\frac{f_{c,\perp}}{\tau_{\text{rel}}} - \frac{f_{c,\perp} - f_{c,\parallel}}{\tau_{\text{iso}}}. \quad (3)$$

In the optical regime and at a negligible doping level, the carrier occupation in the valence band is given by  $f_v = 1 - f_c$ . For both components, we adopt an azimuthal shape following the angular dependence of the off-axis carrier-field coupling matrix elements (for linear polarization) within the Dirac cones, i.e., the total carrier distribution is given by  $f_c(\varphi, t) = f_{c,\parallel}(t) \sin^2 \varphi + f_{c,\perp}(t) \cos^2 \varphi$  [see the inset in Fig. 1(a) for the definition of  $\varphi$ ] [20]. Thereby, considering the limiting case of optical excitation pulses much shorter than the relevant

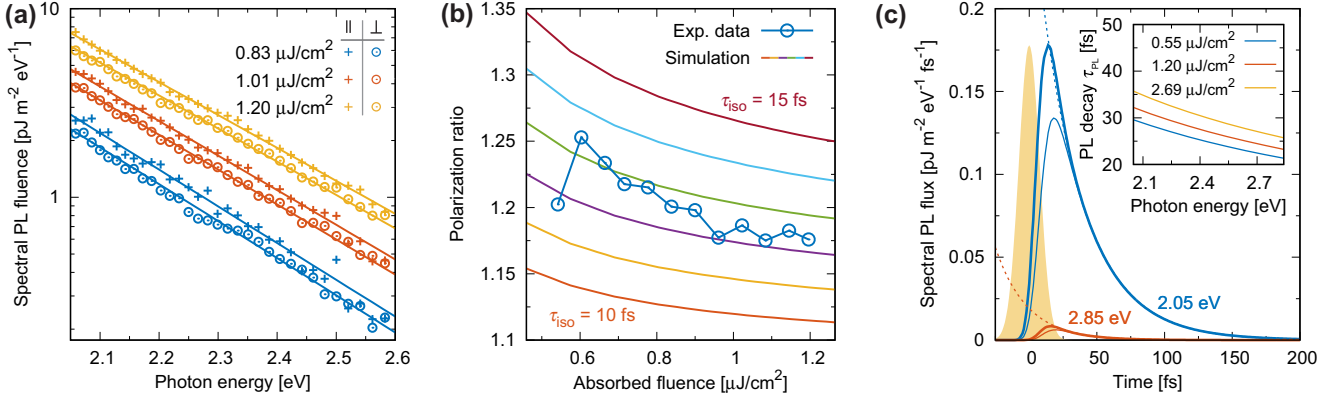


FIG. 2. (a) Comparison of experimentally obtained PL spectra (data points) with results of the microscopic simulations (solid lines). The absolute PL emission fluence is obtained from the simulations. (b) Photon energy-averaged data of the polarization ratio as a function of absorbed fluence. Simulation results are shown for a set of isotropization times between 10 and 15 fs in comparison with experimental data. (c) Simulated PL flux transients at an absorbed fluence of  $1.20 \mu\text{J}/\text{cm}^2$  for the lowest and the highest PL photon energies accessible in the experiment (thick line: parallel PL; thin line: perpendicular PL;  $\tau_{\text{iso}} = 12.5 \text{ fs}$ ). The temporal shape of the pump pulse is shown for comparison (shaded area). Monoexponential fits starting from the right-hand inflection point of the emission curves (dashed lines) determine the effective PL lifetime  $\tau_{\text{PL}}$ . Inset: Effective PL lifetime  $\tau_{\text{PL}}$  for different absorbed fluences.

relaxation times, the perpendicular component  $f_{c,\perp}$  of the carrier distribution is initially zero, and is only populated subsequently due to the azimuthal momentum relaxation term.

Taking into account the azimuthal momentum distribution of both components, the temporally integrated PL flux and polarization ratio are deduced from the evolution of the carrier distribution [19,50] (see Supplemental Material [45]). The time constant  $\tau_{\text{rel}}$  describes the decay of the occupation in the high-energy tail of the carrier distribution and is directly related to the PL lifetime ( $\tau_{\text{PL}} = \tau_{\text{rel}}/2$ ) due to the PL flux scaling quadratically with the occupation [51]. In this model, the polarization ratio is only a function of  $\tau_{\text{PL}}/\tau_{\text{iso}}$ , and the experimentally observed maximum polarization ratio of  $R \approx 1.25$  [cf. Figs. 1(b) and 1(c)] is obtained for  $\tau_{\text{PL}}/\tau_{\text{iso}} \approx 4$ .

In order to quantitatively analyze the experimental data, we combine the rate equations introduced above with a microscopic carrier scattering model. Specifically, in Eqs. (2) and (3), we consider energy-dependent carrier distribution functions  $f_{c,\parallel}(\varepsilon, t)$  and  $f_{c,\perp}(\varepsilon, t)$ , and replace the phenomenological exponential decay (described by  $\tau_{\text{rel}}$ ) by Boltzmann rate equations, which include optical pulse absorption [19,20], Auger and non-Auger carrier-carrier scattering [52–54], as well as carrier-phonon scattering with the relevant optical phonon branches [44,47,55,56]. Both azimuthal populations possess half of the angularly integrated density of states  $D_{\parallel}(\varepsilon) = D_{\perp}(\varepsilon) = D(\varepsilon)/2 = |\varepsilon|/\pi\hbar^2 v_F^2$ , where  $v_F$  is the Fermi velocity [57]. This approach not only provides for a realistic description of carrier relaxation, but also gives direct access to the spectral shape of the PL emission. (See Supplemental Material for a detailed description of the numerical approach [45].) It should be noted that the incoherent PL due to radiative carrier-carrier recombination described in the microscopic modeling may be accompanied by a recently proposed broadband coherent contribution [50], which would be inherently polarized. However, we experimentally verified that the PL detected in our experiment is a fully incoherent emission originating from a nonequilibrium carrier population, and the contribution of off-diagonal elements of the carrier density matrix can be neglected [58].

Results of the microscopic simulations are depicted in Fig. 2(a) (solid lines) in comparison with experimental PL spectra (data points) for three exemplary absorbed fluences. In the simulation, the spectral shape is well reproduced by adopting absorbed fluences of  $0.83\text{--}1.20 \mu\text{J}/\text{cm}^2$  for the experimental incident fluence range of  $82\text{--}117 \mu\text{J}/\text{cm}^2$ . Within the experimental uncertainties, the corresponding graphene absorbance agrees with reported values in the literature [18,59]. The simulated PL spectral flux for an absorbed fluence of  $1.20 \mu\text{J}/\text{cm}^2$  results in a quantum efficiency of  $3 \times 10^{-10}$ , close to the experimental value of  $\sim 10^{-10}$ , which was derived from the PL intensity by taking into account an estimated total detection efficiency of 1%–2% in the considered photon energy range (2.05–2.85 eV).

Figure 2(b) shows a comparison of experimental data for the polarization ratio with simulated curves for a set of isotropization times, each averaged over the experimentally accessible photon energy interval. The time-integrated polarization ratio extracted from the numerical simulations increases with decreasing absorbed fluence and increasing isotropization time. A similar fluence dependence was observed in transient spectroscopy experiments [24]. Considering the experimentally observed polarization ratio, we obtain a fluence- and photon energy-averaged value of  $\tau_{\text{iso}} = 12 \pm 2 \text{ fs}$ . For comparison, in Ref. [39], the authors predict the formation of an isotropic electron distribution within 50 fs at comparable excitation fluences, while initial indications of momentum relaxation are observed after 10 fs. Notably, at photon energies in the meV range, the lifetime of the anisotropic carrier distribution was reported to exceed 1 ps [27].

For comparison with our phenomenological model [cf. Eqs. (2) and (3)], we also extract the effective PL lifetime  $\tau_{\text{PL}}$  from the simulated time-resolved PL emission in a photon energy- and fluence-resolved manner using a monoexponential model [see Fig. 2(c)]. Values of  $\tau_{\text{PL}}$  obtained from the fits are depicted in the inset, exhibiting a slower PL decay at low photon energies and for increasing excitation levels, respectively. For the experimental parameters, the estimated  $\tau_{\text{PL}}$  ranges from 21 to 32 fs. Thus, we obtain a ratio  $\tau_{\text{PL}}/\tau_{\text{iso}}$

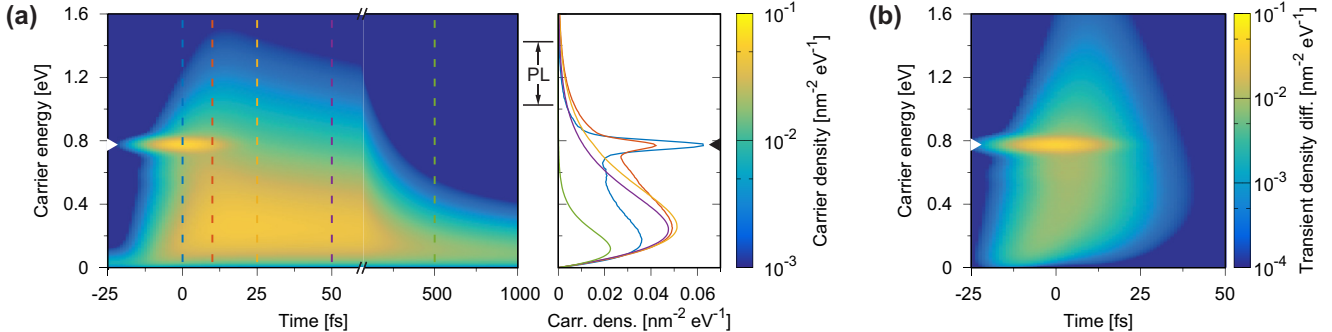


FIG. 3. (a) Time-resolved carrier density map of the parallel component  $D_{\parallel} f_{c,\parallel}$  at an absorbed fluence of  $1.20 \mu\text{J}/\text{cm}^2$  ( $\tau_{\text{iso}} = 12.5 \text{ fs}$ ). Lineouts show the carrier distribution at times of 0, 10, 25, 50, and 500 fs. The carrier energy range accessible by PL spectroscopy in our experiment is indicated. (b) Transient carrier density difference  $D_{\parallel} f_{c,\parallel} - D_{\perp} f_{c,\perp}$  for the same parameters as in (a).

of 1.8 to 2.7, which is in reasonable agreement with the factor of 4 obtained from the simplified, phenomenological model [cf. Fig. 1(c)]. Furthermore, the fluence dependence of  $\tau_{\text{PL}}$  qualitatively accounts for the experimentally observed PL polarization decrease at high fluences, as, in this case, the PL emission contains larger contributions from the isotropic carrier distribution at later times. In addition, from the photon energy dependence of  $\tau_{\text{PL}}$ , a pronounced increase of the polarization ratio for shorter PL wavelengths is expected, which, however, is not observed experimentally.

To obtain further insights into the temporal evolution of graphene excitation underlying anisotropic PL emission, Fig. 3(a) displays the numerically calculated carrier density map  $D_{\parallel} f_{c,\parallel}$  within the first picosecond after optical excitation. During pulse absorption, a pronounced occupation builds up at half the pump photon energy (indicated by the arrow). Carrier-carrier scattering results in a fast fading of the initial occupation peak and a pronounced broadening of the carrier distribution within the first ten femtoseconds. The emerging high-energy tail is the source of the experimentally observed PL. Slower carrier-phonon-mediated carrier cooling on a 100 fs time scale [44,55] quenches PL emission. Figure 3(b) depicts the difference in carrier densities between the parallel and perpendicular components, illustrating the filling of  $D_{\perp} f_{c,\perp}$  due to equienergetic azimuthal scattering. Notably, both energetic broadening and momentum isotropization take place on a time scale comparable to the duration of the pump pulses. Specifically, the transient carrier density difference promptly increases at early delay times, and the carrier anisotropy has almost vanished again after 25 fs.

We note that complementary insights into carrier relaxation can be obtained from transport measurements [60]. While intrinsic relaxation processes, specifically carrier-carrier and carrier-phonon scattering, dominate the high-energy relaxation processes investigated here, electric transport is often limited by impurity scattering close to the Fermi energy [61]. However, scattering with optical phonons has shown to be effective in the high-current limit [62]. Experimentally obtained transport relaxation times range from 15 to 500 fs [63,64].

Finally, we want to point out the connection between the experimentally observed PL polarization ratio  $R$  and the quantum mechanical pseudospin degrees of freedom in graphene. Considering graphene's optical matrix elements [19], one arrives

at the following connection between  $R$  and the expectation values of the sublattice pseudospin in  $q_x$  and  $q_y$  directions,

$$R(E) = \frac{[\langle q | \hat{\sigma}_y | q \rangle]^2}{[\langle q | \hat{\sigma}_x | q \rangle]^2}. \quad (4)$$

Here,  $\hat{\sigma}_x$  and  $\hat{\sigma}_y$  are the pseudospin operators and  $|q\rangle$  is the electron state with momentum  $q$  (relative to the  $K$  and  $K'$  points).  $[\cdot]$  denotes the temporal average over the occupied conduction electron states at energy  $\varepsilon(q) = E/2$ , i.e.,  $[\cdot] = \int dt \sum_q f_c^\varepsilon \delta(\varepsilon - E/2)$ . Thereby, the degree of polarization in the PL spectrum in graphene gives a direct fingerprint of the nonequilibrium pseudospin alignment on ultrashort time scales. However, the sublattice pseudospin alignment in graphene is relatively short lived in comparison to valley pseudospin polarizations in TMDCs. Facilitated by strong spin-orbit coupling, valley lifetimes in, e.g., single-layer MoS<sub>2</sub> lie in the range of a few to hundreds of picoseconds [6], and may even be extended to the nanosecond regime by chemical treatment [65]. Graphene, on the other hand, represents a challenging playground to explore fundamental pseudospin physics on ultrashort time scales in a highly symmetric material.

In summary, we presented polarization-resolved PL spectroscopy as a robust tool to directly access anisotropic carrier distributions in graphene during the first 10–20 fs after ultrashort optical excitation. In combination with a microscopic Boltzmann simulation, we extract a characteristic isotropization time scale of  $12 \pm 2 \text{ fs}$ , resulting in a rapid loss of initial pseudospin alignment imprinted by the optical field.

The authors thank H. K. Yu and M. Maiti for chemical vapor deposition (CVD) preparation, and S. Dechert for Raman characterization of the examined graphene samples. Poly(methyl methacrylate) (PMMA) spin coating and reactive-ion etching were conducted with support by S. Schweda and M. Sivis, respectively. Discussions with S. Yalunin regarding the analytical solution of carrier-carrier scattering integrals are thankfully acknowledged. Partial funding was provided by the Deutsche Forschungsgemeinschaft (DFG-SFB 1073, Project No. A05). T.D. gratefully acknowledges a scholarship by the German Academic Scholarship Foundation.

T.D. and A.N. contributed equally to this work.

- [1] S. A. Wolf, D. D. Awschalom, R. A. Buhrman, J. M. Daughton, S. von Molnár, M. L. Roukes, A. Y. Chtchelkanova, and D. M. Treger, *Science* **294**, 1488 (2001).
- [2] I. Žutić, J. Fabian, and S. Das Sarma, *Rev. Mod. Phys.* **76**, 323 (2004).
- [3] W. Han, R. K. Kawakami, M. Gmitra, and J. Fabian, *Nat. Nanotechnol.* **9**, 794 (2014).
- [4] M. Mecklenburg and B. C. Regan, *Phys. Rev. Lett.* **106**, 116803 (2011).
- [5] D. Song, V. Paltoglou, S. Liu, Y. Zhu, D. Gallardo, L. Tang, J. Xu, M. Ablowitz, N. K. Efremidis, and Z. Chen, *Nat. Commun.* **6**, 6272 (2015).
- [6] X. Xu, W. Yao, D. Xiao, and T. F. Heinz, *Nat. Phys.* **10**, 343 (2014).
- [7] J. R. Schaibley, H. Yu, G. Clark, P. Rivera, J. S. Ross, K. L. Seyler, W. Yao, and X. Xu, *Nat. Rev. Mater.* **1**, 16055 (2016).
- [8] T. Cao, G. Wang, W. Han, H. Ye, C. Zhu, J. Shi, Q. Niu, P. Tan, E. Wang, B. Liu, and J. Feng, *Nat. Commun.* **3**, 887 (2012).
- [9] H. Zeng, J. Dai, W. Yao, D. Xiao, and X. Cui, *Nat. Nanotechnol.* **7**, 490 (2012).
- [10] K. F. Mak, K. L. McGill, J. Park, and P. L. McEuen, *Science* **344**, 1489 (2014).
- [11] D. Xiao, G.-B. Liu, W. Feng, X. Xu, and W. Yao, *Phys. Rev. Lett.* **108**, 196802 (2012).
- [12] A. Srivastava, M. Sidler, A. V. Allain, D. S. Lembke, A. Kis, and A. Imamoğlu, *Nat. Phys.* **11**, 141 (2015).
- [13] A. K. Geim and K. S. Novoselov, *Nat. Mater.* **6**, 183 (2007).
- [14] D. Pesin and A. H. MacDonald, *Nat. Mater.* **11**, 409 (2012).
- [15] O. Klein, *Z. Phys.* **53**, 157 (1929).
- [16] M. I. Katsnelson, K. S. Novoselov, and A. K. Geim, *Nat. Phys.* **2**, 620 (2006).
- [17] A. F. Young and P. Kim, *Nat. Phys.* **5**, 222 (2009).
- [18] R. R. Nair, P. Blake, A. N. Grigorenko, K. S. Novoselov, T. J. Booth, T. Stauber, N. M. R. Peres, and A. K. Geim, *Science* **320**, 1308 (2008).
- [19] M. Mecklenburg, J. Woo, and B. C. Regan, *Phys. Rev. B* **81**, 245401 (2010).
- [20] E. Malic, T. Winzer, E. Bobkin, and A. Knorr, *Phys. Rev. B* **84**, 205406 (2011).
- [21] K. Chen, H. Li, L.-P. Ma, W. Ren, J.-Y. Zhou, H.-M. Cheng, and T. Lai, *J. Appl. Phys.* **115**, 203701 (2014).
- [22] M. Mittendorff, T. Winzer, E. Malic, A. Knorr, C. Berger, W. A. de Heer, H. Schneider, M. Helm, and S. Winnerl, *Nano Lett.* **14**, 1504 (2014).
- [23] X.-Q. Yan, J. Yao, Z.-B. Liu, X. Zhao, X.-D. Chen, C. Gao, W. Xin, Y. Chen, and J.-G. Tian, *Phys. Rev. B* **90**, 134308 (2014).
- [24] M. Trushin, A. Grupp, G. Soavi, A. Budweg, D. De Fazio, U. Sassi, A. Lombardo, A. C. Ferrari, W. Belzig, A. Leitenstorfer, and D. Brida, *Phys. Rev. B* **92**, 165429 (2015).
- [25] J. Yao, X. Zhao, X.-Q. Yan, C. Gao, X.-D. Chen, W. Xin, Y. Chen, Z.-B. Liu, and J.-G. Tian, *Opt. Mater. Express* **5**, 1550 (2015).
- [26] J. Yao, X. Zhao, X.-Q. Yan, X.-T. Kong, C. Gao, X.-D. Chen, Y. Chen, Z.-B. Liu, and J.-G. Tian, *Opt. Express* **23**, 24177 (2015).
- [27] J. C. König-Otto, M. Mittendorff, T. Winzer, F. Kadi, E. Malic, A. Knorr, C. Berger, W. A. de Heer, A. Pashkin, H. Schneider, M. Helm, and S. Winnerl, *Phys. Rev. Lett.* **117**, 087401 (2016).
- [28] X.-Q. Yan, F. Liu, X.-T. Kong, J. Yao, X. Zhao, Z.-B. Liu, and J.-G. Tian, *J. Opt. Soc. Am. B* **34**, 218 (2017).
- [29] J. M. Dawlaty, S. Shivaraman, M. Chandrashekhar, F. Rana, and M. G. Spencer, *Appl. Phys. Lett.* **92**, 042116 (2008).
- [30] P. A. George, J. Strait, J. Dawlaty, S. Shivaraman, M. Chandrashekhar, F. Rana, and M. G. Spencer, *Nano Lett.* **8**, 4248 (2008).
- [31] D. Sun, Z.-K. Wu, C. Divin, X. Li, C. Berger, W. A. de Heer, P. N. First, and T. B. Norris, *Phys. Rev. Lett.* **101**, 157402 (2008).
- [32] R. W. Newson, J. Dean, B. Schmidt, and H. M. van Driel, *Opt. Express* **17**, 2326 (2009).
- [33] M. Breusing, S. Kuehn, T. Winzer, E. Malić, F. Milde, N. Severin, J. P. Rabe, C. Ropers, A. Knorr, and T. Elsaesser, *Phys. Rev. B* **83**, 153410 (2011).
- [34] S. Winnerl, M. Orlita, P. Plochocka, P. Kossacki, M. Potemski, T. Winzer, E. Malic, A. Knorr, M. Sprinkle, C. Berger, W. A. de Heer, H. Schneider, and M. Helm, *Phys. Rev. Lett.* **107**, 237401 (2011).
- [35] S. Tani, F. Blanchard, and K. Tanaka, *Phys. Rev. Lett.* **109**, 166603 (2012).
- [36] D. Brida, A. Tomadin, C. Manzoni, Y. J. Kim, A. Lombardo, S. Milana, R. R. Nair, K. S. Novoselov, A. C. Ferrari, G. Cerullo, and M. Polini, *Nat. Commun.* **4**, 1987 (2013).
- [37] L. M. Malard, K. F. Mak, A. H. Castro Neto, N. M. R. Peres, and T. F. Heinz, *New J. Phys.* **15**, 015009 (2013).
- [38] S. Winnerl, F. Göttfert, M. Mittendorff, H. Schneider, M. Helm, T. Winzer, E. Malic, A. Knorr, M. Orlita, M. Potemski, M. Sprinkle, C. Berger, and W. A. de Heer, *J. Phys.: Condens. Matter* **25**, 054202 (2013).
- [39] E. Malic, T. Winzer, and A. Knorr, *Appl. Phys. Lett.* **101**, 213110 (2012).
- [40] C. H. Lui, K. F. Mak, J. Shan, and T. F. Heinz, *Phys. Rev. Lett.* **105**, 127404 (2010).
- [41] W.-T. Liu, S. W. Wu, P. J. Schuck, M. Salmeron, Y. R. Shen, and F. Wang, *Phys. Rev. B* **82**, 081408 (2010).
- [42] R. J. Stöhr, R. Kolesov, J. Pflaum, and J. Wrachtrup, *Phys. Rev. B* **82**, 121408 (2010).
- [43] T. Koyama, Y. Ito, K. Yoshida, M. Tsuji, H. Ago, H. Kishida, and A. Nakamura, *ACS Nano* **7**, 2335 (2013).
- [44] T. Kampfrath, L. Perfetti, F. Schapper, C. Frischkorn, and M. Wolf, *Phys. Rev. Lett.* **95**, 187403 (2005).
- [45] See Supplemental Material at <http://link.aps.org/supplemental/10.1103/PhysRevB.95.241412>, which includes Refs. [66–77], for a detailed description of the experimental setup, of the sample preparation procedure, and of the theoretical fundamentals of the microscopic simulations.
- [46] N. Bonini, M. Lazzeri, N. Marzari, and F. Mauri, *Phys. Rev. Lett.* **99**, 176802 (2007).
- [47] K. Kang, D. Abdula, D. G. Cahill, and M. Shim, *Phys. Rev. B* **81**, 165405 (2010).
- [48] S. Schäfer, W. Liang, and A. H. Zewail, *New J. Phys.* **13**, 063030 (2011).
- [49] R. P. Chatelain, V. R. Morrison, B. L. M. Klarenaar, and B. J. Siwick, *Phys. Rev. Lett.* **113**, 235502 (2014).
- [50] T. Winzer, R. Ciesielski, M. Handloser, A. Comin, A. Hartschuh, and E. Malic, *Nano Lett.* **15**, 1141 (2015).
- [51] It should be noted that  $\tau_{PL}$  is completely dominated by nonradiative energetic carrier relaxation, and does not correspond to the intrinsic radiative lifetime of excited carriers in graphene (which is typically on the order of picoseconds [54,78]).
- [52] X. Li, E. A. Barry, J. M. Zavada, M. B. Nardelli, and K. W. Kim, *Appl. Phys. Lett.* **97**, 082101 (2010).

- [53] R. Kim, V. Perebeinos, and P. Avouris, *Phys. Rev. B* **84**, 075449 (2011).
- [54] F. Rana, *Phys. Rev. B* **76**, 155431 (2007).
- [55] S. Butscher, F. Milde, M. Hirtschulz, E. Malić, and A. Knorr, *Appl. Phys. Lett.* **91**, 203103 (2007).
- [56] W.-K. Tse and S. Das Sarma, *Phys. Rev. B* **79**, 235406 (2009).
- [57] A. H. Castro Neto, F. Guinea, N. M. R. Peres, K. S. Novoselov, and A. K. Geim, *Rev. Mod. Phys.* **81**, 109 (2009).
- [58] J. H. Gaida, T. Danz, S. Schäfer, and C. Ropers (unpublished).
- [59] D. J. Merthe and V. V. Kresin, *Phys. Rev. B* **94**, 205439 (2016).
- [60] S. Das Sarma, S. Adam, E. H. Hwang, and E. Rossi, *Rev. Mod. Phys.* **83**, 407 (2011).
- [61] F. Chen, J. Xia, and N. Tao, *Nano Lett.* **9**, 1621 (2009).
- [62] A. Barreiro, M. Lazzeri, J. Moser, F. Mauri, and A. Bachtold, *Phys. Rev. Lett.* **103**, 076601 (2009).
- [63] Y.-W. Tan, Y. Zhang, K. Bolotin, Y. Zhao, S. Adam, E. H. Hwang, S. Das Sarma, H. L. Stormer, and P. Kim, *Phys. Rev. Lett.* **99**, 246803 (2007).
- [64] M. Monteverde, C. Ojeda-Aristizabal, R. Weil, K. Bennaceur, M. Ferrier, S. Guéron, C. Glattli, H. Bouchiat, J. N. Fuchs, and D. L. Maslov, *Phys. Rev. Lett.* **104**, 126801 (2010).
- [65] M. Amani, D.-H. Lien, D. Kiriya, J. Xiao, A. Azcatl, J. Noh, S. R. Madhvapathy, R. Addou, S. KC, M. Dubey, K. Cho, R. M. Wallace, S.-C. Lee, J.-H. He, J. W. Ager, X. Zhang, E. Yablonovitch, and A. Javey, *Science* **350**, 1065 (2015).
- [66] X. Li, W. Cai, J. An, S. Kim, J. Nah, D. Yang, R. Piner, A. Velamakanni, I. Jung, E. Tutuc, S. K. Banerjee, L. Colombo, and R. S. Ruoff, *Science* **324**, 1312 (2009).
- [67] M. Gulde, S. Schweda, G. Storeck, M. Maiti, H. K. Yu, A. M. Wodtke, S. Schäfer, and C. Ropers, *Science* **345**, 200 (2014).
- [68] C. Mattevi, H. Kim, and M. Chhowalla, *J. Mater. Chem.* **21**, 3324 (2011).
- [69] Q. H. Wang, Z. Jin, K. K. Kim, A. J. Hilmer, G. L. C. Paulus, C.-J. Shih, M.-H. Ham, J. D. Sanchez-Yamagishi, K. Watanabe, T. Taniguchi, J. Kong, P. Jarillo-Herrero, and M. S. Strano, *Nat. Chem.* **4**, 724 (2012).
- [70] A. C. Ferrari, J. C. Meyer, V. Scardaci, C. Casiraghi, M. Lazzeri, F. Mauri, S. Piscanec, D. Jiang, K. S. Novoselov, S. Roth, and A. K. Geim, *Phys. Rev. Lett.* **97**, 187401 (2006).
- [71] L. M. Malard, M. A. Pimenta, G. Dresselhaus, and M. S. Dresselhaus, *Phys. Rep.* **473**, 51 (2009).
- [72] J. M. Ziman, *Electrons and Phonons* (Oxford University Press, London, 1960).
- [73] R. Saito, G. Dresselhaus, and M. S. Dresselhaus, *Physical Properties of Carbon Nanotubes* (Imperial College Press, London, 1998).
- [74] A. Grüneis, R. Saito, G. G. Samsonidze, T. Kimura, M. A. Pimenta, A. Jorio, A. G. Souza Filho, G. Dresselhaus, and M. S. Dresselhaus, *Phys. Rev. B* **67**, 165402 (2003).
- [75] E. Fermi, *Nuclear Physics*, 4th ed. (The University of Chicago Press, Chicago, IL, 1953).
- [76] A. Mošková and M. Moško, *Phys. Rev. B* **49**, 7443 (1994).
- [77] E. H. Hwang and S. Das Sarma, *Phys. Rev. B* **75**, 205418 (2007).
- [78] T. Limmer, J. Feldmann, and E. Da Como, *Phys. Rev. Lett.* **110**, 217406 (2013).